doi:10.1016/j.jmb.2004.05.074 J. Mol. Biol. (2004) 341, 389–403

JMB

Available online at www.sciencedirect.com

SCIENCE DIRECT®

ELSEVIER

Terbium-mediated Footprinting Probes a Catalytic Conformational Switch in the Antigenomic Hepatitis Delta Virus Ribozyme

Dinari A. Harris, Rebecca A. Tinsley and Nils G. Walter*

Department of Chemistry
The University of Michigan
930 N. University, Ann Arbor
MI 48109-1055, USA

The two forms of the hepatitis delta virus ribozyme are derived from the genomic and antigenomic RNA strands of the human hepatitis delta virus (HDV), where they serve a crucial role in pathogen replication by catalyzing site-specific self-cleavage reactions. The HDV ribozyme requires divalent metal ions for formation of its tertiary structure, consisting of a tight double-nested pseudoknot, and for efficient self- (or *cis*-) cleavage. Comparison of recently solved crystal structures of the cleavage precursor and 3′ product indicates that a significant conformational switch is required for catalysis by the genomic HDV ribozyme. Here, we have used the lanthanide metal ion terbium(III) to footprint the precursor and product solution structures of the *cis*-acting antigenomic HDV ribozyme. Inhibitory Tb^{3+} binds with high affinity to similar sites on RNA as Mg^{2+} and subsequently promotes slow backbone scission. We find subtle, yet significant differences in the terbium(III) footprinting pattern between the precursor and product forms of the antigenomic HDV ribozyme, consistent with differences in conformation as observed in the crystal structures of the genomic ribozyme. In addition, UV melting profiles provide evidence for a less tight tertiary structure in the precursor. In both the precursor and product we observe high-affinity terbium(III) binding sites in joining sequence J4/2 ($Tb_{1/2} \approx 4$ μM) and loop L3, which are key structural components forming the catalytic core of the HDV ribozyme, as well as in several single-stranded regions such as J1/2 and the L4 tetraloop ($Tb_{1/2} \approx 50$ μM). Sensitized luminescence spectroscopy confirms that there are at least two affinity classes of Tb^{3+} binding sites. Our results thus demonstrate that a significant conformational change accompanies catalysis in the antigenomic HDV ribozyme in solution, similar to the catalytic conformational switch observed in crystals of the genomic form, and that structural and perhaps catalytic metal ions bind close to the catalytic core.

Keywords: catalytic RNA folding; melting curve; metal ion binding site; reaction mechanism; terbium luminescence

*Corresponding author

Introduction

RNA enzymes or ribozymes require multivalent metal ions for optimal activity. Structural and biochemical studies have revealed that particularly divalent metal ions play a role in promoting folding of a ribozyme and often directly participate in catalysis. Since structure and dynamics dictate function, the structural and catalytic roles of metal ions have proven to be difficult to dissect, especially since the vast majority of divalent metal ions are bound diffusely, thus facilitating tertiary structure formation by neutralizing and bridging the negatively charged phosphoribose backbone. Recently, there have been major advances in our understanding of the intimate link between

Abbreviations used: HDV, hepatitis delta virus; NMR, nuclear magnetic resonance; rNTPs, ribonucleoside triphosphates; T_m, melting temperature.

E-mail address of the corresponding author: nwalter@umich.edu

metal ion binding and RNA function.[1–5] Many of these studies have utilized the class of "small" ribozymes, which includes the hammerhead, hairpin, hepatitis delta virus (HDV), and *Neurospora* Varkud satellite (VS) ribozymes. These ribozymes are classified by their relatively small size (less than 200 nucleotides) and common reaction chemistry; however, they are structurally diverse and have different metal ion requirements (or specificities). Particularly, in the past few years the HDV ribozyme has received considerable attention and has redefined our understanding of how RNA enzymes work.

The hepatitis delta virus is a satellite RNA of the human hepatitis B virus (HBV).[6] Co-infection of patients with both HBV and HDV results in more severe forms of hepatitis, including liver cirrhosis, and can lead to death. During viral replication, both the ~1700 nucleotides long genomic RNA and its complement, the antigenomic RNA, undergo self-cleavage reactions catalyzed by internal ribozyme motifs that are absolutely essential for propagation of the virus *in vivo*.[7,8] These self-cleavage activities reside within contiguous ~85 nucleotide sequence elements that form similar double-nested pseudoknots, the genomic and antigenomic forms of the HDV ribozyme.[9] In the presence of divalent cations, the HDV ribozyme undergoes self-cleavage *in vitro*, during which deprotonation of a specific 2′-OH group and nucleophilic attack on the adjacent scissile phosphate result in formation of 2′,3′-cyclic phosphate and 5′-OH termini. The crystal structure of the self-cleaved genomic form revealed for the first time that the ribozyme adopts a tight tertiary structure by forming the two base-pair helix P1.1 between loop L3 and the joiner sequence J1/4, creating a pair of nested pseudoknots, which buries the active site in a deep cleft.[10] Thus, the cleavage site resides in close proximity to the catalytically important cytosine 75/76 (C75 in the genomic ribozyme, C76 in the antigenomic ribozyme) (Figure 1). This observation inspired biochemical studies that found C75/76 to be directly involved in reaction chemistry as a general base or acid, thereby opening our eyes to the fact that RNA is not solely dependent on the functional capabilities of divalent metal ions to perform catalysis.[11–14]

Refinement of the crystal structure of the self-cleaved genomic HDV ribozyme located 12 divalent metal ions throughout the structure, yet none of them was found in proximity to the proposed catalytic core.[15] A possible explanation for this lack of metal ions in the active site is that the crystallized sequence lacks the scissile phosphate and the nucleophilic 2′-OH group, which both could serve as metal binding ligands. This observation is consistent with biochemical data suggesting that the 5′ sequence upstream of the cleavage site, although not obviously interacting with the 3′ product sequence, has a significant impact on catalytic activity. For example, kinetic

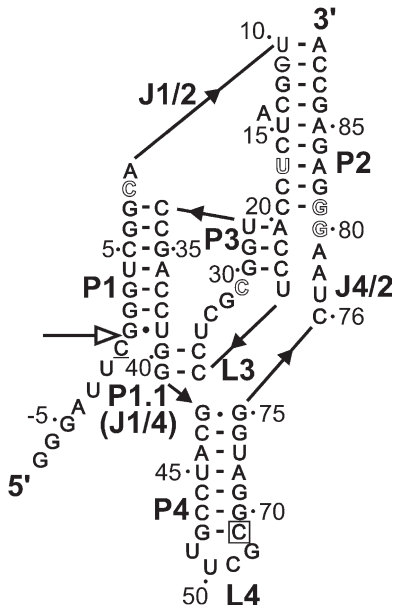

Figure 1. Secondary structure of the *cis*-acting antigenomic HDV ribozyme used in this study. The noncleavable precursor form was generated by modifying the 2′-OH group of the underlined nucleotide 5′ to the cleavage site (open arrow) to 2′-methoxy during chemical synthesis. In order to maintain the previously defined antigenomic numbering system in our P4-truncated ribozyme, we renumbered the nucleotides downstream of the L4 loop. The boxed cytosine residue at the bottom of P4 is defined as residue 69. Outlined are the five nucleotides for which we observe the largest (>twofold) change in normalized scission intensity between the precursor and product forms of the antigenomic ribozyme.

studies of a *trans*-acting HDV ribozyme have suggested that components of the substrate immediately 5′ to the cleavage site destabilize ground-state substrate binding and thereby lower the activation free energy barrier of cleavage.[16] This result, in conjunction with the observation that the active site cleft in the product crystal structure is deep and tightly packed, thus not obviously providing a trajectory for substrate exit, has led to the proposal that the 5′ sequence may be accommodated by straining (bending) of the substrate and/or loosening of the catalytic core.[9,17] In support of this notion, fluorescence spectroscopy studies have recently shown that a *trans*-acting HDV ribozyme undergoes both substantial global and local conformational rearrangements upon catalysis.[17–19] In addition, NMR spectroscopy has provided further evidence for structural differences between the precursor and product forms of *trans*-acting HDV ribozymes.[20,21] Most recently, Doudna and co-workers have succeeded in crystallizing several forms of the genomic *cis*-acting precursor ribozyme.[22] Comparison with the product structure reveals that an important conformational change accompanies and, in fact, appears to facilitate HDV ribozyme cleavage. Consistent with the biochemical data, the precursor crystal structure depicts an outer-sphere coordinated divalent

metal ion in an active site pocket formed by loop L3. This metal ion is lost from the active site together with the 5′ sequence as the catalytic conformational switch occurs, which prevents the product form of the genomic HDV ribozyme from catalyzing the reverse ligation reaction.[22]

To address the questions of whether a similar conformational switch accompanies catalysis in the antigenomic HDV ribozyme and what form it takes outside of a crystal lattice, we have utilized terbium(III)-mediated footprinting as a probe of secondary and tertiary structure as well as metal binding properties in *cis*-acting precursor and product forms in solution. The lanthanide metal ion terbium(III) has previously been found to be a powerful probe of RNA tertiary structure at nucleotide resolution, as well as of metal ion binding sites in RNA. Tb^{3+} binds to similar sites on the polyanionic RNA as Mg^{2+}, with an affinity two to four orders of magnitude higher.[23–25] The inhibitory terbium(III) has the ability to substitute for magnesium(II) because Tb^{3+} has an ionic radius (0.92 Å) similar to that of Mg^{2+} (0.72 Å), and they share the same preference for coordination to oxygen ligands.[23,24,26] Once bound to RNA, the transiently deprotonated aqua complex $Tb(OH)(aq)^{2+}$ abstracts protons from nearby 2′-OH groups, which allows for nucleophilic attack of the resulting 2′ oxyanion on the juxtaposed phosphodiester, leading to slow local strand scission 3′ to a given nucleotide.[23,24,27,28] Tb^{3+} can effectively catalyze scission of an RNA backbone at physiologic pH due to its lower pK_a (~7.9) compared to that of Mg^{2+} (11.4).[23,24,29] By systematically varying the Tb^{3+} concentration, it is possible to obtain a footprint of secondary and tertiary structure (at millimolar $[Tb^{3+}]$) and a map of metal-binding sites (at micromolar $[Tb^{3+}]$).[23,24] Our terbium(III) footprinting patterns indicate that the precursor and product forms of the *cis*-acting antigenomic HDV ribozyme are similar in overall conformation but indeed show distinctions in several key regions, consistent with the differences observed in the crystal structures of the genomic ribozyme. In addition, UV melting profiles provide evidence for a less tight tertiary structure in the precursor. We also map high-affinity terbium(III) binding sites to J4/2 ($Tb_{1/2} \approx 4$ μM), the joiner sequence that contains the catalytic C76, and to loop L3, found in the precursor crystal structure to bind the potentially catalytic metal ion. Sensitized luminescence spectroscopy confirms that there are at least two different affinity classes of Tb^{3+} binding sites. Our data are thus consistent with the notion that a significant conformational change leads to catalysis in the *cis*-cleaving antigenomic HDV ribozyme in solution, similar to that proposed for the genomic ribozyme, and that structural and perhaps catalytic metal ions bind close to the catalytic core.

Table 1. Self-cleavage activity of the antigenomic HDV ribozyme used in this study

Metal ion conditions	Cleavage rate (k_{obs}) (min^{-1})	Cleavage extent (%)
11 mM Mg^{2+}, 0 mM Tb^{3+}	43.0 ± 4.6	72 ± 2
11 mM Mg^{2+}, 5 mM Tb^{3+}	44.4 ± 5.9	27 ± 2

Results

Terbium(III) inhibits the HDV ribozyme, probably by competing with cations that support catalysis

The lanthanide metal terbium(III) has proven to be a versatile probe of both metal binding as well as secondary and tertiary structure of RNA. In addition, the luminescent properties of Tb^{3+} provide for a facile means of measuring metal-binding affinity. It has long been known that Tb^{3+} replaces Mg^{2+} as an RNA ligand of much higher affinity, which as a result usually inhibits catalysis, for example in the hammerhead[30] and hairpin ribozymes.[23] In previous work we found that cleavage in a *trans*-acting HDV ribozyme was significantly inhibited in the presence of terbium(III),[19] so that we felt compelled to investigate the impact that terbium(III) has on catalysis in a *cis*-acting HDV ribozyme. The HDV ribozyme used here (Figure 1) is slightly modified from a previously described antigenomic HDV ribozyme.[13] Our construct differs from the latter wild-type antigenomic HDV sequence in that the sequence upstream of U-3 was modified to 5′-GGGA-3′ for optimal *in vitro* transcription of the self-cleaving RNA, and in that P4 was truncated and capped with a stable UUCG tetraloop to limit the total length to 80 nucleotides for chemical synthesis and introduction of a 2′-methoxy modification at the cleavage site to structurally study a non-cleavable precursor.

First, we tested the single-turnover cleavage activity of our *cis*-acting antigenomic HDV ribozyme in the presence and absence of 5 mM $TbCl_3$, which is the highest concentration used in the terbium(III)-mediated footprinting assays. As expected, we found terbium(III) to be an inhibitor of catalysis. Specifically, self-cleavage of the pre-annealed precursor ribozyme under standard conditions (25 mM acetic acid, 25 mM Mes, 50 mM Tris–HCl (pH 7.5), at 37 °C) was initiated by the addition of Mg^{2+} to a final concentration of 11 mM (Materials and Methods), showing that the conversion of precursor to product follows first-order kinetics, with an observed rate constant k_{obs} of 43.0(±4.6) min^{-1} and a 72(±2)% extent of cleavage (Table 1). This finding is in good agreement with reported values of $k_{obs} = 31\ min^{-1}$ and 77% cleavage extent for the wild-type antigenomic HDV ribozyme sequence,[31] indicating that our sequence modifications do not interfere with catalysis. When the reaction was initiated by the addition of a mixture of Mg^{2+} and Tb^{3+} (final concentrations 11 mM and 5 mM, respectively), k_{obs} was unaffected (44.4(±5.9) min^{-1}); however, the extent of

cleavage was significantly lowered to 27(±2)%. Such a lowered cleavage amplitude in the presence of terbium(III) was also observed with the hairpin ribozyme, but the mechanism of this type of inhibition is not well understood.[23,30]

Terbium(III) footprinting reveals subtle structural differences between the precursor and product at nucleotide resolution

High (millimolar) concentrations of terbium(III) have previously been used to slowly cut an RNA phosphodiester backbone in a largely sequence-independent manner, preferentially in single-stranded or non-Watson–Crick base-paired regions, thus generating a footprint of the RNA's secondary and tertiary structure at nucleotide resolution.[19,23–26,29,32–37] In addition, due to the strongly electrostatic interactions of the highly charged Tb^{3+} with the polyanionic RNA backbone, scission is particularly enhanced on RNA surfaces of high local charge density, revealing potential metal binding sites at low (micromolar) concentration of terbium(III).[19,24,27,37] Because of its near-physiologic aqueous pK_a of 7.9 and its Mg^{2+} and Ca^{2+}-like coordination properties with a preference for oxygen ligands, terbium(III) has recently become popular as an alternative to Mg^{2+} and Pb^{2+}-induced footprinting.[24,25] We therefore set out to utilize Tb^{3+} to probe and compare the structures of the precursor and product forms of our antigenomic HDV ribozyme in solution.

To this end, trace amounts of the radiolabeled non-cleavable precursor or product form of our antigenomic HDV ribozyme were prefolded under standard conditions in the presence of 11 mM Mg^{2+}, as described in Materials and Methods, followed by addition of increasing concentrations of Tb^{3+} (from 1 μM to 5 mM) to initiate slow backbone scission at 37 °C over one hour (under these conditions, only a small fraction of RNA is cleaved, avoiding secondary hits on an already cut RNA molecule). The footprinting patterns of the precursor and product (Figures 2 and 3) show similarities with respect to their protected and susceptible regions, which is consistent with the fact that the precursor and product forms of the antigenomic HDV ribozyme share an overall similar conformation. In particular, both scission patterns are consistent with the expected secondary structure

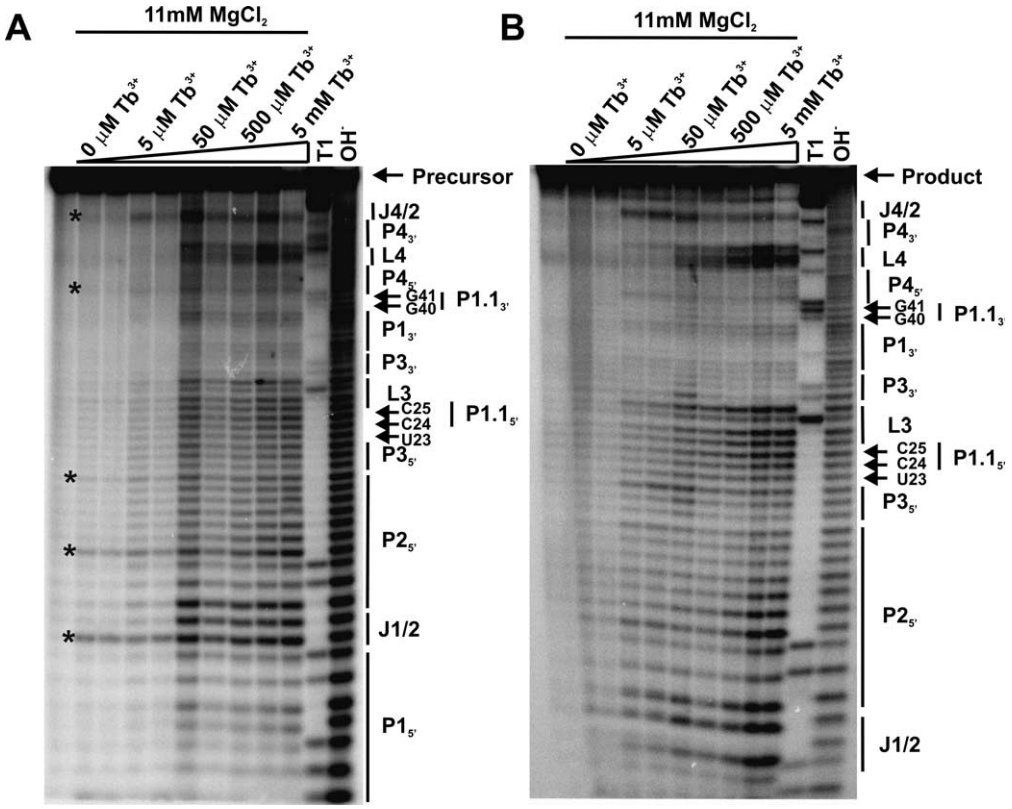

Figure 2. Terbium(III)-mediated footprinting of 5′-^{32}P-labeled antigenomic HDV ribozyme. A, Precursor footprint after incubation for one hour in 25 mM acetic acid, 25 mM Mes, 50 mM Tris–HCl (pH 7.5), 11 mM $MgCl_2$, at 37 °C (see Materials and Methods). From left to right: lane 1, radiolabeling precursor without incubation; lanes 2–10, samples incubated with increasing Tb^{3+} concentrations (0, 0.001, 0.005, 0.01, 0.05, 0.1, 0.5, 1, and 5 mM), as indicated; lanes 11 and 12, G-specific RNase T_1 and alkaline hydrolysis (OH^-) ladders, respectively. Note that significant scission occurs in J4/2, L3, J1/2, and P4 at low micromolar Tb^{3+} concentrations, which is indicative of high-affinity metal binding. As the Tb^{3+} concentration is increased, backbone scission becomes more intense. Scission occurs 3′ to the indicated nucleotide. Asterisks indicate background scission in 5′-UpA-3′ and 5′-CpA-3′ steps. B, Product footprint under identical conditions and with a similar lane arrangement as in A.

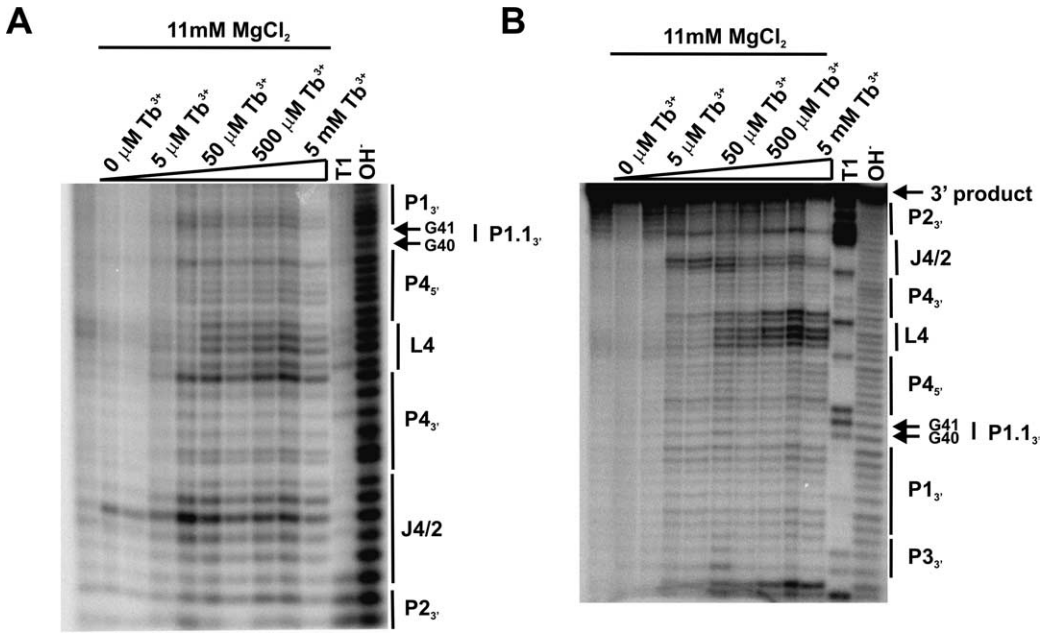

Figure 3. Terbium(III)-mediated footprinting, resolving the 3′-end of the antigenomic HDV ribozyme. A, The 3′-end-labeled precursor after incubation for one hour in 25 mM acetic acid, 25 mM Mes, 50 mM Tris–HCl (pH 7.5), 11 mM $MgCl_2$, at 37 °C (see Materials and Methods). From left to right: lane 1, radiolabeling precursor without incubation; lanes 2–10, samples incubated with increasing Tb^{3+} concentrations (0, 0.001, 0.005, 0.01, 0.05, 0.1, 0.5, 1, and 5 mM), as indicated; lanes 11 and 12, G-specific RNase T_1 and alkaline hydrolysis (OH^-) ladders, respectively. Note that scission occurs 5′ to the indicated nucleotide. B, Footprint of 5′-end-labeled product, in which the gel was run longer than in Figure 2B to better resolve the 3′ end. Conditions and lane arrangement were similar as in A, but scission occurs 3′ to the indicated nucleotide.

of the HDV ribozyme; relative protection is observed in all five Watson–Crick base-paired stems, P1–P4 and P1.1; while strong scission is observed in the backbone of loops L3 and L4 as well as in joiners J1/2 and J4/2 (Figures 2 and 3).

Interestingly, the precursor (as well as product) consistently show significant backbone scission, even in the absence of Tb^{3+}, 3′ to C_8 (J1/2), C_{13}, C_{19} ($P2_{5'}$), C_{43} ($P4_{5'}$), and U_{77} (J4/2) (marked by asterisks in Figure 2A). Further inspection revealed that these nucleotides represent the five sequence elements of the type 5′-CpA-3′ or 5′-UpA-3′ present in our antigenomic HDV ribozyme. Previous studies have shown that the phosphodiester bonds of 5′-UpA-3′ and 5′-CpA-3′ sequence elements are >100-fold and up to 35-fold more reactive, respectively, at physiologic pH and temperature than those of other dinucleotide steps.[38] A possible explanation is a distinct hydration pattern around the scissile phosphate, attacking 2′-OH and neighboring bases that, by hydrogen bonding, lowers the transition state barrier for scission in these sequence elements.[38,39] In our quantitative analysis, we therefore normalized against the no-Tb^{3+} background (Materials and Methods), thus correcting for this background scission in the absence of Tb^{3+}. Still, terbium(III) induces additional phosphodiester bond scission 3′ to C_8 and U_{77}, as detailed in the following.

Figure 4A summarizes the relative percentage of RNA cut at each resolved nucleotide of the precursor and product forms at 5 mM Tb^{3+} (top and bottom, respectively). These patterns were consistently observed on altogether 11 sequencing gels resolving either the 5′ or 3′ ends of the precursor and 16 gels resolving either the 5′ or 3′ ends of the product. Interestingly, under all concentrations of terbium(III) tested, the histogram plots of the precursor reveal more even scission intensities than those of the product. By comparison, the histogram plots of the product appear more rugged. There are two potential explanations for this effect: (1) a technical one in that the footprinting gels of the precursor appeared to typically have more of a smear to them, somewhat evening out the intensities; (2) a structural one in that the precursor HDV ribozyme structure may be considerably more dynamic than the product structure, so that terbium(III) footprinting results in an overall averaging of a broader variety of structures. This latter explanation is consistent with the idea that the precursor structure must be more dynamic (loose) to accommodate the 5′ sequence extension and is further supported by differences in the precursor and product melting profiles (see below).

Footprinting at high Tb^{3+} concentrations generates a direct map of secondary and tertiary structure, as scission in Watson–Crick base-paired regions such as P3 is suppressed relative to that in single-stranded regions. A concentration of 5 mM Tb^{3+} in the precursor induces strong scission at (or 3′ to) U4-C5 ($P1_{5'}$), A9 (J1/2), U10-C18 ($P2_{5'}$),

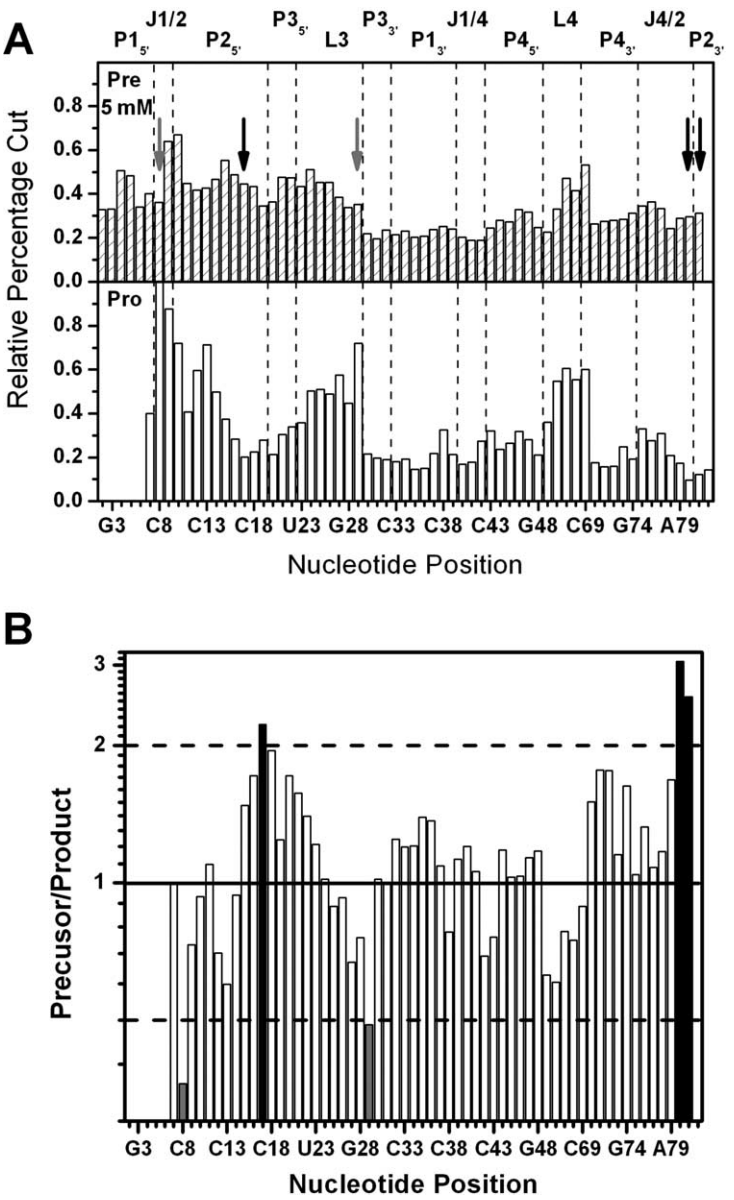

Figure 4. Quantification of terbium(III)-induced backbone scission of the antigenomic HDV ribozyme. A, Histogram plots of precursor (Pre; striped bars; top) and product (Pro; open bars; bottom) showing the relative percent scission 3′ to each resolved nucleotide when incubating the RNA with 5 mM Tb^{3+}. The relative percentage cut was calculated as detailed in Materials and Methods and additionally normalized to the most intensely hit nucleotide, C8 of the product at 5 mM Tb^{3+}, for a relative comparison. Gray arrows indicate an increase in scission intensity by >twofold from precursor to product, while black arrows indicate a decrease in scission intensity by >twofold in the same direction. B, Histogram plot showing the relative change in scission intensity from precursor to product, expressed as ratio between the normalized intensities in A. Continuous horizontal line, no change (ratio = 1); broken horizontal lines, twofold change; gray bars, increase in scission >twofold from precursor to product; black bars, decrease in scission intensity by >twofold in the same direction.

C21-C22 ($P3_{5'}$), U23-U26 (L3), C51-G52 (L4), and C69 ($P4_{3'}$). The product in the presence of 5 mM Tb^{3+} shows strong scission at C8-A9 (J1/2), U10, C13 ($P2_{5'}$), C29 (L3) and moderate scission at G12, A14 ($P2_{5'}$), C24-G28 (L3), U50-G52 (L4), and C69 ($P4_{3'}$). In Figure 4A we have highlighted by arrows those five nucleotides, C8, U17, C29, G80, and G81, that show a more than twofold change in normalized scission intensity between the precursor and product; Figure 4B shows the ratio of precursor over product scission intensity for all positions. Please note that C8 and C29 (gray) increase in scission intensity after cleavage, while U17, G80, and G81 decrease (black). The terbium(III)-mediated footprinting patterns of the precursor and product HDV ribozyme thus are subtly, but noticeably distinct, consistent with the idea that their global structures are not identical. Our results therefore support previous evidence from fluorescence resonance energy transfer,[17] 2-aminopurine fluorescence quenching,[18] NMR spectroscopy,[20,21] and terbium(III)-mediated footprinting[19] that have revealed structural differences between the precursor and product forms of *trans*-acting HDV ribozymes. Here, we have derived specifics of structural rearrangements in the *cis*-acting antigenomic HDV ribozyme at nucleotide resolution that can be compared with recent crystal structures of precursor and product forms of the genomic HDV ribozyme, which provide evidence for a significant and catalytically essential conformational switch in the active site.[22]

High-affinity terbium binding sites are located near the catalytic core of the HDV ribozyme

One of the most striking observations in the terbium(III)-mediated scission patterns of both the precursor and product antigenomic HDV ribozyme is the significant scission at micromolar

concentrations of Tb^{3+}, indicative of high-affinity terbium(III) binding sites, in joining sequence J4/2 and loop L3, which are key structural components forming the catalytic core of the HDV ribozyme, as well as in other single-stranded regions such as J1/2 and the L4 tetraloop (Figures 2 and 3). Particularly scission in J4/2, comprising nucleotides G75, the catalytic C76, and U77, starts to become visible at only 5 μM Tb^{3+}, indicating a high-affinity, apparently non-specific outer-sphere metal ion binding site in this region. By comparison, the high-affinity Tb^{3+} binding site involving the L4 tetraloop (including U49-G52 and C69; see Figure 1) seems to be of slightly lower affinity than the site in J4/2 (Figures 2 and 3).

To more quantitatively compare these two high-affinity Tb^{3+} binding sites, the relative percentage of scission in these regions was summed, normalized (Materials and Methods), and plotted against the Tb^{3+} concentration (Figure 5). The titration curves in the J4/2 region of the precursor and product forms of our antigenomic HDV ribozyme have an interesting characteristic. As the concentration of Tb^{3+} increases, the intensity of scission increases up to 50 μM Tb^{3+}, while further titration results in a significant decrease in relative scission intensity. This relative "protection" from terbium(III) scission may be due to a terbium(III)-induced structural perturbation, as it coincides with a shift in relative scission intensity from U77 > C76 > G75 to C76 > U77 > G75 (see, for example, Figure 3B). A similar "protection" effect was observed above 100 μM Tb^{3+} in the footprinting of $tRNA^{Lys,3}$.[32] The concentration of Tb^{3+} required for half-maximal scission intensity in J4/2 ($Tb_{1/2}$) was calculated based on the initial rise and gave similar values of 5 μM and 3 μM for the precursor and product forms, respectively, of our *cis*-acting antigenomic HDV ribozyme (Figure 5A and B). (It should be noted that these values are lower estimates for $Tb_{1/2}$, due to overlap with the decrease at higher Tb^{3+} concentration.) Such a high affinity of the joiner sequence J4/2 for terbium(III) is consistent with calculations of the surface charge potential[19,40] and with the observation of a metal ion binding site in J4/2, along with several peripheral binding sites in J1/2 and at the bottom of P2, in the refined product crystal structure of the genomic HDV ribozyme.[15]

The other region of high affinity for Tb^{3+} for which we were able to derive quantitative information is the L4 tetraloop region (comprising

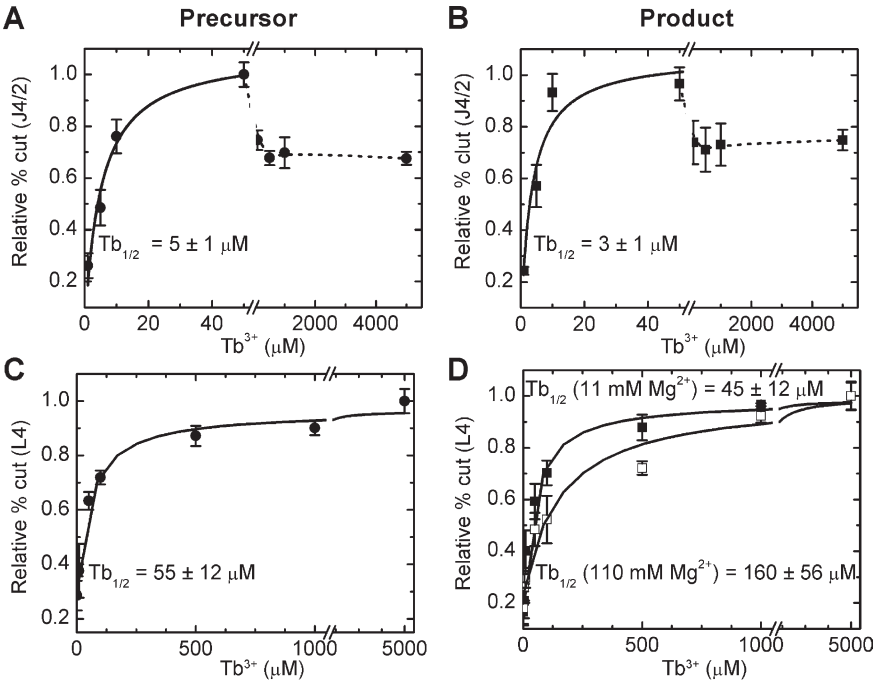

Figure 5. Tb^{3+} affinity of joiner J4/2 and tetraloop L4 in the antigenomic HDV ribozyme. A, Tb^{3+} concentration dependence of terbium(III)-induced backbone scission of joiner J4/2, comprising nucleotides G75, C76, and U77 (Figure 1), in the precursor. The relative percentage cut was calculated as detailed in Materials and Methods, averaged for four separate gels, and additionally normalized to the highest scission intensity (here reached at 50 μM Tb^{3+}). Continuous line, fit to a Hill equation, yielding the indicated apparent terbium(III) dissociation constant. Broken line, a Tb^{3+}-induced structural change at higher Tb^{3+} concentrations leads to a relative decrease in terbium(III)-induced scission intensity. B, Tb^{3+} concentration dependence of terbium(III)-induced backbone scission of joiner J4/2 in the product, analyzed as described in A. C, Tb^{3+} concentration dependence of terbium(III)-induced backbone scission of tetraloop L4, comprising nucleotides U49-G52 and C69 (Figure 1), in the precursor, analyzed as described for A. D, Tb^{3+} concentration dependence of terbium(III)-induced backbone scission of tetraloop L4 in the product, analyzed as described for A. Increasing the Mg^{2+} concentration from 11 mM (■) to 110 mM (□) significantly reduces the Tb^{3+} affinity (i.e. increases the apparent terbium(III) dissociation constant), as indicated.

U49-G52 and C69). As shown in Figure 4C and D, a continuous rise in backbone scission with increasing Tb^{3+} concentration is observed in both the precursor and product, respectively. We found $Tb_{1/2}$ to be 55 μM and 45 μM for the precursor and the product, respectively, indicating an ~tenfold lower Tb^{3+} affinity than that of J4/2. Interestingly, scission at nucleotides U49 and G52 in both precursor and product at 5 mM Tb^{3+} (where secondary structure formation is enhanced) is slightly weaker than that of nucleotides U50, C51, and C69 (see Figures 3 and 4B), consistent with NMR and crystal structures that depict these two nucleotides engaged in a *trans*-wobble G-U base-pair.[41–43] However, neither the NMR nor crystal structures resolve any bound multivalents, perhaps due to the fact that the NMR structure was determined in low ionic strength (50 mM NaCl) devoid of multivalents, while the crystal structure was solved in high monovalent (2 M NH_4^+, 50 mM K^+), possibly preventing binding of the low concentration of divalent present (1.5 mM Mg^{2+}). To confirm that our terbium(III) scission site in the UUCG tetraloop indeed represents a high-affinity, low-specificity multivalent metal ion binding site, we performed the Tb^{3+}-mediated footprinting in the presence of 110 mM instead of 11 mM Mg^{2+}. While the terbium(III) scission patterns of precursor and product at 110 mM Mg^{2+} were nearly identical with those at 11 mM Mg^{2+} (data not shown), $Tb_{1/2}$ for loop L4 increased from 45 μM to 160 μM upon raising the [Mg^{2+}] tenfold from 11 mM to 110 mM (Figure 4D). This change compares surprisingly well with the fivefold increase in $Tb_{1/2}$ observed in terbium(III) footprinting of the suspected Mg^{2+} binding region of the P4 region in RNase P, when raising the [Mg^{2+}] tenfold from 15 mM to 150 mM Mg^{2+}.[36]

The *cis*-acting HDV ribozyme binds terbium(III) with higher affinity than a *trans*-acting HDV ribozyme

In addition to the use of Tb^{3+} as a probe of metal binding and secondary/tertiary structure, its distinctive spectroscopic properties allow this lanthanide ion to be used to investigate metal binding of the entire RNA structure. Although terbium has a small extinction coefficient of direct absorption, upon binding proximal to chromophores it can emit sensitized luminescence. Such a case occurs when terbium(III) ions bind to RNA where nearby excited guanine bases transfer their energy to the lanthanide ion. Using this unique property, the metal ion binding characteristics of the hammerhead and hairpin ribozymes have recently been probed.[23,44] Here, we set out to examine, by sensitized luminescence spectroscopy, the binding affinity of terbium(III) to the product form of our *cis*-acting antigenomic HDV ribozyme and compare this affinity to that of the previously characterized *trans*-acting HDV ribozyme.[19] (Due to the relatively high RNA concentrations needed for these measurements (1 μM) we were unable to perform Tb^{3+} titrations of the synthetic non-cleavable *cis*-acting precursor form.)

Addition of 100 μM Tb^{3+} to 1 μM product form of the pre-annealed antigenomic HDV ribozyme under standard conditions in 11 mM Mg^{2+} and excitation at 290 nm (Materials and Methods) resulted in the emission spectrum of Figure 6A (continuous line), revealing a terbium(III)-specific signal with four peaks, the most intense of which is centered around 545 nm. In the absence of RNA, no such spectrum is observed (Figure 6A, broken line). Upon terbium(III) titration, the emission at 545 nm increases significantly before saturating above 70 μM Tb^{3+}. The resulting curve is best fit to the sum of two independent Hill equations (Materials and Methods), providing for two apparent dissociation constants ($Tb_{1/2}$) of 15 μM and 42 μM (Figure 6B), suggesting that at least two classes of terbium binding sites or modes exist. Strikingly, these two $Tb_{1/2}$ values compare well with the estimates for Tb^{3+} binding affinity derived from footprinting of the J4/2 ($Tb_{1/2} = 3$ μM) and L4 ($Tb_{1/2} = 45$ μM) regions (Figure 5). Furthermore, comparing these values obtained from Tb^{3+} titration of the product form of our *cis*-acting HDV ribozyme to those previously obtained for the product complex of a

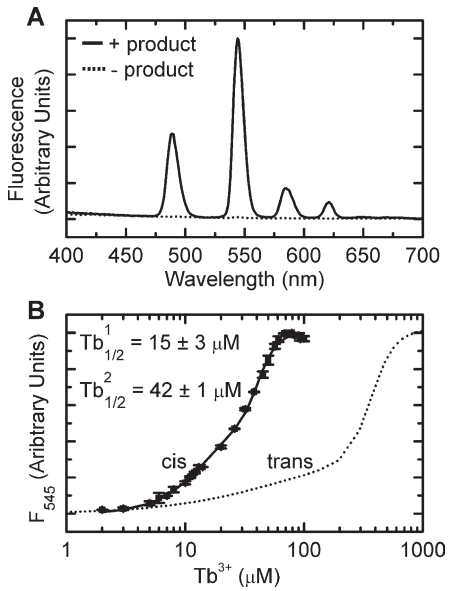

Figure 6. Sensitized luminescence spectroscopy of 1 μM product form of the *cis*-acting antigenomic HDV ribozyme upon Tb^{3+} titration. A, Fluorescence emission spectrum of the product prefolded in 11 mM Mg^{2+} (Materials and Methods), in the presence (continuous line) and absence (broken line) of 100 μM Tb^{3+}. B, Fluorescence titration of the product with terbium(III) in the presence of 11 mM Mg^{2+} (Materials and Methods). Data were fit to a sum of two independent Hill equations to yield two apparent Tb(III) dissociation constants $Tb_{1/2}$ as indicated and Hill constants of $n1 = 2.0$ and $n2 = 6.1$, respectively. For comparison, data from a similar titration of a *trans*-acting ribozyme are shown (broken line).[19]

trans-cleaving ribozyme, 70 μM and 340 μM,[19] we find an ~five- to eightfold higher terbium(III) binding affinity in the *cis*-acting ribozyme (Figure 6B). This higher affinity for multivalents is possibly linked to the ~30-fold faster cleavage rate constant of our *cis*-acting ribozyme compared to the *trans*-acting one under similar conditions ($43\ min^{-1}$ (Table 1) *versus* $1.34\ min^{-1}$ [18] in 11 mM Mg^{2+} (pH 7.5), at 37 °C), which is consistently observed when severing the J1/2 and/or L4 connections (Figure 1) to obtain a *trans*-acting construct.[9]

Thermal melting curves confirm tertiary structural differences between the precursor and product forms

To complement our terbium(III)-mediated footprinting data with global structural information, thermal UV-melting profiles were acquired under standard conditions (11 mM Mg^{2+}, pH 7.5) for the non-cleavable precursor and product forms of the *cis*-acting antigenomic HDV ribozyme (Materials and Methods). Both the precursor and product exhibit two distinct folding transitions that have nearly the same melting temperatures (T_m) for the two RNAs. In the precursor the first transition (T_{m1}) occurs at 62 °C and the second transition (T_{m2}) at 84 °C, while in the product the transitions occur at 64 °C (T_{m1}) and 83 °C (T_{m2}) (Figure 7). The partial unfolding around T_{m1} is most likely due to loss of some tertiary interactions, while the higher melting temperature, T_{m2}, most likely characterizes loss of secondary structure. Strikingly, while the overall behavior of the precursor and product is quite similar, particularly the lower-temperature transitions have first derivatives of remarkably different full-widths at half-maximum. From this difference we estimate a considerably lower transition enthalpy of $\Delta H = -24.6$ kcal/mol for the precursor compared to $\Delta H = -90.1$ kcal/mol in the product (Figure 7). These observations suggest that the precursor form of the *cis*-acting antigenomic HDV ribozyme has a significantly more dynamic, less cooperative tertiary structure than the product form, consistent with our terbium(III)-mediated footprinting results.

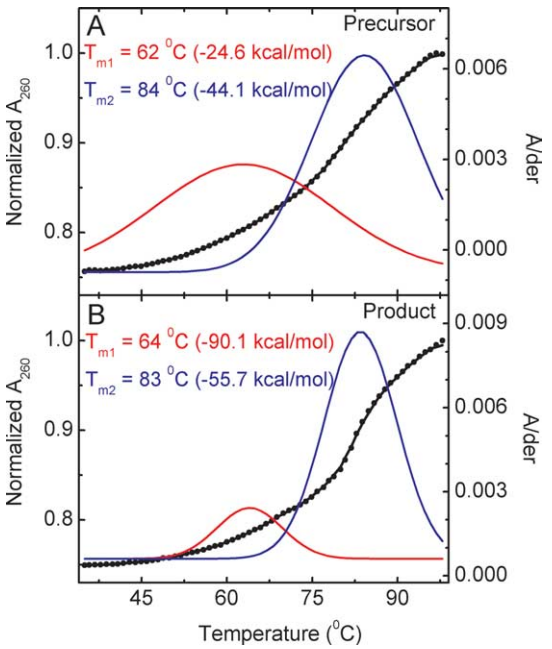

Figure 7. Thermal denaturation of the antigenomic HDV ribozyme in 11 mM Mg^{2+}. A, Melting profile of the precursor. The relative absorbance of the RNA at 260 nm (●, left axis) and a bimodal gaussian distribution fit to the smoothed first derivative (color, right axis) are shown. The melting temperatures T_m and associated transition enthalpies ΔH (in parentheses) for melting of the tertiary and secondary structure of the RNA were determined from the red and blue curves, respectively (Materials and Methods). B, Melting profile of the product, analyzed as described for A.

Discussion

For over 20 years, since the discovery of RNA enzymes, it has been clear that RNA is not just a passive carrier of genetic information. In fact, RNA plays a key role in almost every aspect of cellular metabolism, including protein transport, RNA splicing, peptide bond formation, and regulation of translation.[45–47] Metal ions, particularly divalents, are essential cofactors that aid in forming a fully structured and functional RNA molecule.[1–5] Ribozymes are no exception, as they require metal ions to properly position reactive groups such that they are poised for catalysis, and in some cases to directly participate in reaction chemistry. Deciphering the exact role of these metals has proven quite challenging. The HDV ribozyme is one example of a catalytic RNA that appears to utilize both structural and catalytic metal ions to carry out catalysis. Bevilacqua and co-workers have estimated that the overall rate enhancement by divalent metal ions is ~3000-fold, of which the catalytic contribution is ~25-fold and the remaining larger contribution is chiefly structural in nature.[48] To complement the existing biochemical data, we have used terbium(III)-mediated footprinting to probe the HDV ribozyme's metal ion binding properties as well as secondary and tertiary structure.

Recently, Doudna and co-workers have solved several precursor crystal structures of the genomic HDV ribozyme and have proposed, by comparison with the product crystal structure, that a significant conformational switch controls catalysis by ejecting a catalytically critical divalent metal ion from the active site, thus preventing the 3′ product from catalyzing re-ligation.[22] Using terbium(III)-footprinting in solution, we have observed subtle, yet significant structural differences between the precursor and 3′ product of the other natural HDV ribozyme, the antigenomic form. While the precursor and product are similar in global architecture and share helices P1–P4 and P1.1, they show

structural differences consistent with a conformational switch. Figure 8 identifies the five nucleotides in the genomic precursor and product crystal structures that correspond to those nucleotides for which we observe the largest (>twofold) difference in relative terbium(III)-induced scission intensity in the antigenomic sequence (arrows in Figure 4A; please note that γA8, γC14, and γC26 in the genomic crystal structure have their equivalents in C8, U17, and C29, respectively, in our antigenomic ribozyme; γ is used in the following to distinguish genomic from antigenomic numbering). Importantly, these five nucleotides divide into two different classes (Figure 4A): (1) γC14/U17, G80, and G81 (both G80 and G81 are common to both genomic and antigenomic), which are all located at the bottom of helix P2 (Figures 1 and 8) and for which scission intensity decreases >twofold from precursor to product; and (2) γA8/C8, in joiner J1/2, and γC26/C29, in loop L3, for which scission intensity increases >twofold from precursor to product. The first class of terbium(III)-induced scission sites is located at the exact position, at the bottom of helix P2, where an earlier study found a Mg^{2+}-induced scission site that is correlated with enzymatic activity of a shortened *trans*-acting HDV ribozyme.[49] Combined with the fact that we observe a decrease in terbium(III)-induced scission at this site in the cleavage product, we propose that this is a non-specific metal ion binding site that becomes significantly less populated upon cleavage. Given that it is distant from the cleavage site by >20 Å we further propose that this is an important structural, rather than catalytic, metal binding site in the antigenomic HDV ribozyme.

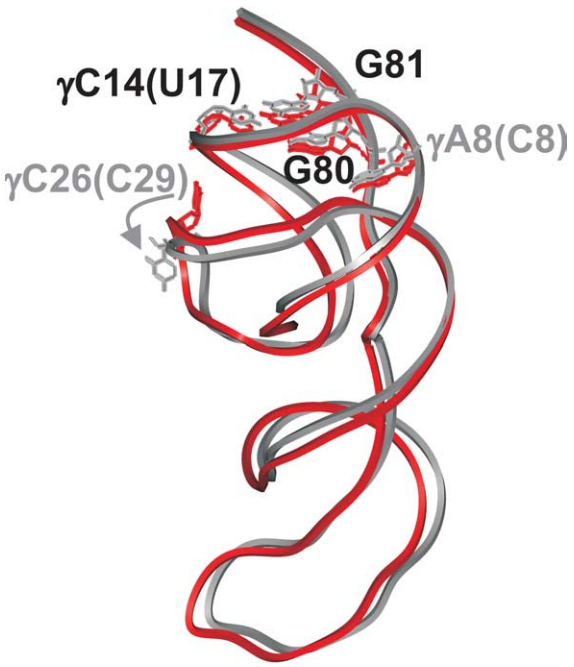

Figure 8. Backbone ribbon representations of the precursor (red, PDB ID 1SJ3) and 3′ product (silver, PDB ID 1CX0) forms of the genomic HDV ribozyme crystal structures. The indicated nucleotides represent the residues corresponding to those in our antigenomic HDV ribozyme with the largest (>twofold) changes in terbium(III)-mediated scission intensity between precursor and product. Interestingly, these sites mark regions that either represent a known metal ion binding site at the bottom of helix P2 (γC14, G80, G81; highlighted in black to indicate, as in Figure 4, a decrease in terbium(III) scission intensity by >twofold from precursor to product) or are implicated in conformational changes accompanying and essential for catalysis (γA8 and γC26; highlighted in gray to indicate, as in Figure 4, an increase in terbium(III) scission intensity by >twofold from precursor to product). Please note that γA8, γC14, and γC26 in the genomic crystal structure have their equivalents in C8, U17, and C29, respectively, in our antigenomic ribozyme (parentheses), while G80 and G81 are shared between the two forms. This Figure was generated using InsightII.

The second class of terbium(III) scission sites is enhanced in the product over the precursor structure and is found in two separate locations that are both implicated in the catalytic conformational switch of the genomic HDV ribozyme (Figure 8).[22] γC26/C29 is part of loop L3 (Figure 1) and is one of the nucleotides that undergo the most dramatic rearrangements upon cleavage in the genomic ribozyme (Figure 8). These rearrangements in L3 inevitably lead to changes in local electrostatics and metal binding properties as well as backbone geometry, thus providing for a plausible explanation for enhanced terbium(III)-induced scission. While γC26/C29 shows the most pronounced enhancement within L3, the loop is generally cut quite strongly and its overall scission pattern exhibits among the most significant changes between precursor and product (Figure 4). Similar observations were made using terbium(III)-mediated footprinting on a *trans*-acting HDV ribozyme.[19] These findings are striking since the available crystallographic evidence implicates L3 in binding of a catalytic divalent metal ion.[22] We therefore propose that L3 provides for a negative electrostatic surface that non-specifically localizes metal ions close to the catalytic site; in case of hydrated divalents, such as Mg^{2+} and Ca^{2+}, this leads to catalysis, while trivalent metal ions such as Tb^{3+} and the $Co(NH_3)_6^{3+}$ complex bind tightly but are not compatible with catalysis.

γA8/C8 in joiner J1/2 also shows enhanced terbium(III)-mediated scission in the product compared to the precursor, yet essentially does not rearrange upon cleavage (Figure 8). To understand this behavior, it is instructive to consider the structural context of this nucleotide; it is part of the strand crossover between helices P1 and P2 that joins the two parallel stacks of the ribozyme, consisting of P1–P1.1–P4 and P2–P3 (Figure 1). γA8/C8 as well as its neighbor A9 (γU9 in the genomic sequence) stack on P1, while U10 (γG10) stacks on P2, leading to a sharp backbone turn between positions 9 and 10.[10,22] While this backbone geometry does not change significantly upon cleavage, the conformational switch accompanying cleavage entails movement of the P1–P1.1–P4 and P2–P3

stacks towards each other as the "wedge" presented by the sequence 5′ to the cleavage site is removed (Figure 8). A similar, yet more pronounced global conformational change has been observed by fluorescence resonance energy transfer (FRET) in a *trans*-acting ribozyme.[17–19,50,51] It is further supported in our *cis*-acting antigenomic HDV ribozyme by the significantly less cooperative tertiary structure melting transition of the precursor compared to the product, from which a nearly 66 kcal/mol less favorable transition enthalpy derives (Figure 7). This global structural change may well alter the structural dynamics or strain around the joining J1/2 sequence in the *cis*-acting ribozyme, thus leading to the observed enhanced susceptibility toward terbium(III) scission after catalysis.

Another region that shows strong susceptibility towards terbium(III)-mediated backbone scission, especially in the product at low Tb^{3+} concentrations, is the joiner J4/2 sequence that contains the catalytic C76 residue. Again, similar observations were made using terbium(III)-mediated footprinting on a *trans*-acting HDV ribozyme.[19] In the *cis*-acting antigenomic ribozyme, the terbium(III) affinity of the J4/2 region is in fact one of the highest reported so far for an RNA,[19,23,26,29,32–37] with $Tb_{1/2} = 5$ μM and 3 μM in the precursor and product, respectively, in a background of 11 mM Mg^{2+} (Figure 5A and B). A similar $Tb_{1/2}$ of 4.2 μM was observed in hammerhead ribozyme HH16 under similar ionic conditions using luminescence titration of Tb(III).[44] Our findings are consistent with Pb^{2+}-induced scission of the genomic cleavage product, which occurs predominantly at C75/76 in J4/2 in the presence of low concentrations of Mg^{2+} and which is suppressed by higher Mg^{2+} concentrations.[52] Furthermore, under basic conditions (pH 9.0) specific cleavage is extended throughout the J4/2 joining region so that cleavage is observed at G74, C75 (major cleavage site) and G76 with Mg^{2+}, Mn^{2+}, or Ca^{2+} (corresponding to our antigenomic G75, C76, U77, respectively).[52] Both the precursor and product crystal structures depict the J4/2 region as a tight trefoil turn with a sharp double-twist in the phosphodiester backbone.[10,22] This unique structural motif projects the catalytic C75/76 deeply into the catalytic core so that it approaches the scissile phosphate, making the trefoil turn a key structural feature essential for formation of the catalytic pocket. In the refined genomic product crystal structure, a Mg^{2+} is resolved that appears to be outer-sphere (i.e. mostly electrostatically) bound to the phosphate of G76 (corresponding to U77 in our antigenomic ribozyme);[15] if this metal ion were replaced by Tb^{3+}, the transiently deprotonated $Tb(OH)(aq)^{2+}$ species may be close enough to deprotonate the 2′-OH of C75/76 (the metal–2′O distance is 4.3 Å[10]), leading to subsequent backbone scission 3′ to C75/76. This is consistent with our observation of terbium(III)-mediated backbone scission with relative intensities of C76 > U77 > G75 in the antigenomic HDV ribozyme (Figure 4A). Since the crystallographic J4/2-bound Mg^{2+} is at a distance of ~9 Å from the scissile phosphate, its major function is likely the structural organization of the essential trefoil motif, not participation in catalysis. It should be noted, however, that inhibition of catalysis by Tb^{3+} or $Co(NH_3)_6^{3+}$ may not necessarily relate to displacement of a catalytically involved divalent by the higher-affinity trivalent metal ion (complex); it is also conceivable that substitution of Tb^{3+} or $Co(NH_3)_6^{3+}$ for an essential structural metal ion, such as those bound to P2 or to joiner J4/2, may result in sufficient perturbation of the sugar-phosphate backbone or base-stacking geometry to render a ribozyme molecule inactive. Such a possibility is supported by the fact that previous structure probing by Pb^{2+} revealed that the formation of P2 directs the overall fold of the ribozyme, specifically the correct formation of L3 and J4/2.[52] This latter finding parallels our data, which suggest significant cooperativity between binding of Tb^{3+} at the bottom of P2 and in J4/2 (Figure 3), which then may render the structure and electrostatics of L3 such that the loop attracts a catalytic metal ion. Also in support of the notion of an effect of terbium(III) on structural rather than catalytic metal ions in RNA, two of the other small ribozymes, the hairpin and hammerhead, are both catalytically highly active in the absence of divalents, thus are not obligatory metallo-enzymes, yet are still strongly inhibited by Tb^{3+}.[23,30,53]

We also observe significant Tb^{3+}-induced scission in the L4 tetraloop of both the precursor and product of our *cis*-acting antigenomic HDV ribozyme, which is suppressed by higher Mg^{2+} concentrations (Figure 5C and D). To our knowledge, this is the first evidence that the ubiquitous UUCG tetraloop, a member of the most frequent and thermodynamically stable UNCG family of tetraloops found in natural RNAs,[54] does in fact bind metal ions with moderate affinity ($Tb_{1/2} \approx 50$ μM in a background of 11 mM Mg^{2+}). High-resolution structures from NMR spectroscopy and X-ray crystallography did not reveal a well-coordinated metal binding site;[41–43] however, metal ion binding may help explain the unusual stability of this tetraloop motif. Our findings complement a recent report on binding of europium(III), another lanthanide metal ion, to the other stable family of tetraloops of type GNRA.[55] It is also interesting to note that the Tb^{3+} affinity of ~50 μM that we find for the UUCG tetraloop is similar to that of the lower-affinity class of Tb^{3+} binding sites observed by sensitized terbium(III) luminescence titration, which appears to represent the largest fraction of terbium(III) binding sites in the *cis*-acting HDV ribozyme (Figure 6).

In summary, the data presented here not only reveal that the *cis*-acting antigenomic HDV ribozyme undergoes a similar conformational switch in solution as has been proposed, based on crystallographic evidence, to enable catalysis in the

genomic form, but they also shed light on locations of metal ions likely to be relevant to proper structure formation and catalysis of the HDV ribozyme. Future studies are needed to address how exactly structural and catalytic metal ions exert their influence on catalysis.

Materials and Methods

Preparation of RNA

The non-cleavable precursor of our antigenomic HDV ribozyme, modified with a 2′-methoxy group at the cleavage site (Figure 1), was chemically synthesized by Dharmacon Research, Inc., and the 2′-orthoester protection groups were removed following the manufacturer's recommendations.[56] Deprotected RNA was purified by C_8 reverse-phase HPLC chromatography with a linear acetonitrile gradient in triethylammonium acetate as described.[57,58] The unmodified self-cleaved product form of the antigenomic HDV ribozyme was generated by run-off transcription from a double-stranded, PCR-amplified template that encoded an upstream T7 promoter. Transcription reactions contained 40 mM Tris–HCl (pH 7.5), 15 mM $MgCl_2$, 5 mM dithiothreitol, 2 mM spermidine, 4 mM each rNTP, five units/ml of inorganic pyrophosphatase, and 0.1 mg/ml of T7 RNA polymerase and were incubated at 37 °C overnight (~16 hours). The self-cleaved full-length transcript was isolated after denaturing, 8 M urea, 10% (w/v) polyacrylamide gel electrophoresis by UV shadowing, diffusion elution of small gel slices, and ethanol-precipitation.

For cleavage reactions, the radiolabeled precursor HDV ribozyme was transcribed as described above, except that 0.04 mCi of [α-^{32}P]GTP and 0.125 μg/μl of a DNA oligonucleotide were added to the reaction mixture. This DNA oligonucleotide has a sequence fully complementary to the 15 nucleotides at the 5′ end of the precursor (G_{-7} to C_8) and was used to increase the yield of the uncleaved precursor RNA.[59] The transcription reaction was incubated for one hour at 37 °C and the RNA fractionated by electrophoresis on an 8 M urea, 10% (w/v) polyacrylamide denaturing gel. Uncleaved precursor RNA was located by autoradiography, excised, eluted into 0.1 mM EDTA, and recovered by ethanol-precipitation. The radiolabeled RNA was stored in 0.1 mM EDTA at −20 °C.

Terbium stock solutions

The highest purity terbium(III) chloride (99.9%) was purchased from Sigma-Aldrich. $TbCl_3$ stock solutions at 100 mM were prepared in 5 mM cacodylate (pH 5.5) and stored in small aliquots at −20 °C to prevent formation of insoluble hydroxide species.

Cleavage assays

Radiolabeled precursor RNA (5–50 nM) was heated to 90 °C for two minutes in a buffer containing 5 mM Tris–HCl (pH 7.5), 0.5 mM spermidine. The precursor was then pre-incubated at 37 °C for ten minutes, after which the reactions were adjusted to the final pH with a buffer containing 25 mM acetic acid, 25 mM Mes, 50 mM Tris–HCl (pH 7.5). These mixtures were incubated for an additional five minutes at 37 °C, followed by addition of 0.25 volumes of a solution (also at 37 °C) containing 55 mM $MgCl_2$ and 0.5 mM spermidine to start the reaction.[13] For cleavage assays performed in the presence of 5 mM Tb^{3+}, the latter solution was supplemented with 25 mM $TbCl_3$. Cleavage kinetics were followed by removing aliquots (5 μl) at specified times and quenching them with 10 μl of 80% (v/v) formamide, 0.025% (w/v) xylene cyanol, 0.025% (w/v) bromophenol blue, and 50 mM EDTA. The reaction product was separated from the precursor by gel electrophoresis under denaturing conditions (8 M urea, 6% (w/v) polyacrylamide gels), quantified, and normalized to the sum of the precursor and product bands using a PhosphorImager Storm 840 with ImageQuant software (Molecular Dynamics). Time traces of product formation were fit to the single-exponential first-order rate equation $y = y_0 + A_1(1 - e^{-t/\tau 1})$, employing Marquardt–Levenberg non-linear least-squares regression (Microcal Origin 7.0), where A_1 is the amplitude and τ^{-1} the pseudo first-order rate constant k_{obs}.

Terbium(III)-mediated footprinting

To observe the slow backbone scission mediated by $Tb(OH)(aq)^{2+}$, purified non-cleavable precursor and self-cleaved product forms of the antigenomic HDV ribozyme were (5′-^{32}P)-phosphorylated with T4 polynucleotide kinase and [γ-^{32}P]ATP and re-purified by denaturing 8 M urea, 10% polyacrylamide gel electrophoresis, followed by diffusion elution, and ethanol-precipitation, as described.[19,23,24] To resolve its 3′ end region the precursor had to be 3′ end labeled using [^{32}P]pCp and T4 RNA ligase, since (5′-^{32}P)-labeling of the precursor did not resolve this region well due to smearing in the gel. The radiolabeled RNA (250,000 cpm per 10 μl reaction volume) was pre-annealed in buffer (5 mM Tris–HCl (pH 7.5), 0.5 mM spermidine), denatured at 90 °C for two minutes, and incubated at 37 °C for ten minutes. To fold the tertiary structure of the RNA, Mg^{2+} was added five minutes prior to the addition of various Tb^{3+} concentrations (1 μM to 5 mM final concentration) and incubated for an additional one hour at 37 °C. The scission reaction was stopped by adding EDTA (pH 8.0), to a final concentration of 50 mM and ethanol-precipitation at −20 °C. The precipitated RNA was redissolved in urea loading buffer (80% formamide, 0.025% xylene cyanol, 0.025% bromophenol blue, 50 mM EDTA, 9 M urea) and analyzed on an 8 M urea, wedged 15% polyacrylamide sequencing gel, alongside sequencing ladders from partial digestion with G-specific RNase T_1 and alkaline hydrolysis as described.[19,23,24] Product bands were either directly visualized using autoradiography or quantified, using a PhosphorImager Storm 840 with ImageQuant software (Molecular Dynamics), and normalized by calculating a relative extent of scission (Π) from the equation:

$$\Pi = \frac{\left(\dfrac{\text{band intensity at nucleotide } x}{\sum_i \text{band intensity at nucleotide } i} \right)_{y\ [Tb^{3+}]}}{\left(\dfrac{\text{band intensity at nucleotide } x}{\sum_i \text{band intensity at nucleotide } i} \right)_{0\ \text{mM}[Tb^{3+}]}}$$

where y is the terbium(III) concentration in a particular scission reaction and x the analyzed nucleotide position

of the RNA. 0 mM [Tb^{3+}] signifies a control reaction incubated in the same fashion as the terbium(III)-containing ones, except that no terbium(III) was added. Normalizing in this way the intensities at the various terbium(III) concentrations to the samples without terbium(III) corrects for any non-specific background degradation. To derive a Tb^{3+} affinity the relative percentage cut was plotted over varying terbium(III) concentrations ([Tb^{3+}]) and fit to a Hill equation, essentially as described:[19,23]

$$y = y_{\max} \frac{[Tb^{3+}]^n}{[Tb^{3+}]^n + Tb_{1/2}^n}$$

to yield an apparent terbium(III) dissociation constant $Tb_{1/2}$ and a cooperativity or Hill constant n.

Terbium(III) luminescence measurements

Steady-state luminescence spectra of terbium(III) bound to the pre-annealed and equilibrated product form of the antigenomic HDV ribozyme (1 μM) in standard reaction buffer (25 mM acetic acid, 25 mM Mes, 50 mM Tris–HCl (pH 7.5), 11 mM $MgCl_2$) at 37 °C were measured on an Aminco-Bowman Series 2 (AB2) spectrofluorometer (Thermo Spectronic), while slowly increasing the Tb^{3+} concentration. The latter was accomplished by adding small aliquots of an identical solution of 1 μM product in 25 mM acetic acid, 25 mM Mes, 50 mM Tris–HCl (pH 7.5), 11 mM $MgCl_2$, but supplemented with 0.4 mM Tb^{3+}, followed by mixing and removal of a solution volume equivalent to that of the added aliquot. This procedure ensures that neither the concentrations of RNA and buffer nor the total solution volume change over the course of the titration. After each titration step, the solution was equilibrated for five minutes until the signal had stabilized, before an emission spectrum was recorded. Excitation was at 290 nm (slit width of 4 nm), while the steady-state emission was scanned with a slit width of 8 nm. To extract the luminescence intensity of the major peak at 545 nm, each peak was fit between 535 nm and 555 nm with a gaussian distribution function:

$$y = y_0 + \frac{A}{W\sqrt{\pi/2}} e^{-2(x-x_0)^2/w^2}$$

to yield the peak height as the pre-exponential factor, from which the background value in the absence of Tb^{3+} was subtracted. These signals were plotted over varying terbium(III) concentrations and were fit to a Hill equation, essentially as described above, to yield an apparent terbium(III) dissociation constant $Tb_{1/2}$ and a cooperativity or Hill constant n. For a fit over the complete terbium(III) titration range, a sum of two independent Hill equations produced the best result, as judged by the χ^2 deviation and the residuals.

Thermal denaturation

Thermal denaturation of 1 μM precursor or product form of the *cis*-acting antigenomic HDV ribozyme was carried out using a Beckman DU-640B UV–Vis spectrophotometer with High Performance Temperature Controller and Micro Auto 6 T_m cell holder. RNA samples (~300 μl) were prepared as described for the cleavage reaction and degassed for five minutes prior to obtaining UV melting curves. Absorbance readings at 260 nm were collected every 1.0 deg.C as the sample was heated from 35 °C to 99 °C at a rate of 0.2 deg.C/minute. Each UV melting curve represents data collected from two melts of freshly prepared RNA. After normalization, the first derivative was determined, smoothed by adjacent averaging, and two melting temperatures were obtained by fitting to two gaussian distributions using MicroCal Origin 7.0. The full-widths at half-maximum of the gaussian distributions yield transition enthalpies from:

$$\Delta H^0 = \frac{B}{\left(\frac{1}{T_1} - \frac{1}{T_2}\right)}$$

where B is −7.00 cal/mol K for this unimolecular melting transition and T_1 and T_2 are the temperatures at half-maximum of the first derivative curve.[60]

Acknowledgements

We thank Jennifer Doudna and Ailong Ke for sharing crystal structure data and a manuscript prior to publication, Stephen Scaringe for synthesizing the 80-mer precursor RNA, and all the members of the Walter laboratory for stimulating discussions and thoughtful suggestions. This work was supported by NIH grant GM62357 to N.G.W., a University of Michigan Rackham Merit predoctoral fellowship to R.A.T. and D.A.H., a pre-doctoral Merck/UNCF fellowship to D.A.H., and an NIH supplement to grant GM62357 to R.A.T.

References

1. Hanna, R. & Doudna, J. A. (2000). Metal ions in ribozyme folding and catalysis. *Curr. Opin. Chem. Biol.* **4**, 166–170.
2. Pyle, A. M. (2002). Metal ions in the structure and function of RNA. *J. Biol. Inorg. Chem.* **7**, 679–690.
3. DeRose, V. (2002). Two decades of RNA catalysis. *Chem. Biol.* **9**, 961–969.
4. Bokinsky, G., Rueda, D., Misra, V. K., Rhodes, M. M., Gordus, A., Babcock, H. P. *et al.* (2003). Single-molecule transition-state analysis of RNA folding. *Proc. Natl Acad. Sci. USA*, **100**, 9302–9307.
5. Draper, D. E. (2004). A guide to ions and RNA structure. *RNA*, **10**, 335–343.
6. Hadziyannis, S. J. (1997). Review: hepatitis delta. *J. Gastroenterol. Hepatol.* **12**, 289–298.
7. Lai, M. M. (1995). The molecular biology of hepatitis delta virus. *Annu. Rev. Biochem.* **64**, 259–286.
8. Macnaughton, T. B., Shi, S. T., Modahl, L. E. & Lai, M. M. (2002). Rolling circle replication of hepatitis delta virus RNA is carried out by two different cellular RNA polymerases. *J. Virol.* **76**, 3920–3927.
9. Shih, I. H. & Been, M. D. (2002). Catalytic strategies of the hepatitis delta virus ribozymes. *Annu. Rev. Biochem.* **71**, 887–917.
10. Ferre-D'Amare, A. R., Zhou, K. & Doudna, J. A. (1998). Crystal structure of a hepatitis delta virus ribozyme. *Nature*, **395**, 567–574.
11. Perrotta, A. T., Shih, I. & Been, M. D. (1999). Imidazole rescue of a cytosine mutation in a self-cleaving ribozyme. *Science*, **286**, 123–126.
12. Nakano, S., Chadalavada, D. M. & Bevilacqua, P. C.

(2000). General acid–base catalysis in the mechanism of a hepatitis delta virus ribozyme. *Science*, **287**, 1493–1497.
13. Wadkins, T. S., Shih, I., Perrotta, A. T. & Been, M. D. (2001). A pH-sensitive RNA tertiary interaction affects self-cleavage activity of the HDV ribozymes in the absence of added divalent metal ion. *J. Mol. Biol.* **305**, 1045–1055.
14. Oyelere, A. K., Kardon, J. R. & Strobel, S. A. (2002). p*K*(a) perturbation in genomic hepatitis delta virus ribozyme catalysis evidenced by nucleotide analogue interference mapping. *Biochemistry*, **41**, 3667–3675.
15. Ferre-D'Amare, A. R. & Doudna, J. A. (2000). Crystallization and structure determination of a hepatitis delta virus ribozyme: use of the RNA-binding protein U1A as a crystallization module. *J. Mol. Biol.* **295**, 541–556.
16. Shih, I. & Been, M. D. (2001). Energetic contribution of non-essential 5′ sequence to catalysis in a hepatitis delta virus ribozyme. *EMBO J.* **20**, 4884–4891.
17. Pereira, M. J., Harris, D. A., Rueda, D. & Walter, N. G. (2002). Reaction pathway of the *trans*-acting hepatitis delta virus ribozyme: a conformational change accompanies catalysis. *Biochemistry*, **41**, 730–740.
18. Harris, D. A., Rueda, D. & Walter, N. G. (2002). Local conformational changes in the catalytic core of the *trans*-acting hepatitis delta virus ribozyme accompany catalysis. *Biochemistry*, **41**, 12051–12061.
19. Jeong, S., Sefcikova, J., Tinsley, R. A., Rueda, D. & Walter, N. G. (2003). Trans-acting hepatitis delta virus ribozyme: catalytic core and global structure are dependent on the 5′ substrate sequence. *Biochemistry*, **42**, 7727–7740.
20. Luptak, A., Ferre-D'Amare, A. R., Zhou, K., Zilm, K. W. & Doudna, J. A. (2001). Direct p*K*(a) measurement of the active-site cytosine in a genomic hepatitis delta virus ribozyme. *J. Am. Chem. Soc.* **123**, 8447–8452.
21. Tanaka, Y., Tagaya, M., Hori, T., Sakamoto, T., Kurihara, Y., Katahira, M. & Uesugi, S. (2002). Cleavage reaction of HDV ribozymes in the presence of Mg2 + is accompanied by a conformational change. *Genes Cells*, **7**, 567–579.
22. Ke, A., Zhou, K., Ding, F., Cate, J. H. & Doudna, J. A. (2004). A conformational switch controls hepatitis delta virus ribozyme catalysis. *Nature*, **429**, 201–205.
23. Walter, N. G., Yang, N. & Burke, J. M. (2000). Probing non-selective cation binding in the hairpin ribozyme with Tb(III). *J. Mol. Biol.* **298**, 539–555.
24. Harris, D. A. & Walter, N. G. (2003). Probing RNA structure and metal-binding sites using terbium footprinting. *Curr. Protocols Nucl. Acid Chem.* **6.8**, 6.8.1–6.8.8.
25. Sigel, R. K. & Pyle, A. M. (2003). Lanthanide ions as probes for metal ions in the structure and catalytic mechanism of ribozymes. *Met. Ions Biol. Syst.* **40**, 477–512.
26. Saito, H. & Suga, H. (2002). Outersphere and innersphere coordinated metal ions in an aminoacyl-tRNA synthetase ribozyme. *Nucl. Acids Res.* **30**, 5151–5159.
27. Ciesiolka, J., Marciniec, T. & Krzyzosiak, W. (1989). Probing the environment of lanthanide binding sites in yeast tRNA(Phe) by specific metal-ion-promoted cleavages. *Eur. J. Biochem.* **182**, 445–450.
28. Matsumura, K. & Komiyama, M. (1997). Enormously fast RNA hydrolysis by lanthanide(III) ions under physiological conditions: eminent candidates for novel tools of biotechnology. *J. Biochem.* **122**, 387–394.
29. Sigel, R. K., Vaidya, A. & Pyle, A. M. (2000). Metal ion binding sites in a group II intron core. *Nature Struct. Biol.* **7**, 1111–1116.
30. Feig, A. L., Scott, W. G. & Uhlenbeck, O. C. (1998). Inhibition of the hammerhead ribozyme cleavage reaction by site-specific binding of Tb. *Science*, **279**, 81–84.
31. Wadkins, T. S., Perrotta, A. T., Ferre-D'Amare, A. R., Doudna, J. A. & Been, M. D. (1999). A nested double pseudoknot is required for self-cleavage activity of both the genomic and antigenomic hepatitis delta virus ribozymes. *RNA*, **5**, 720–727.
32. Hargittai, M. R. & Musier-Forsyth, K. (2000). Use of terbium as a probe of tRNA tertiary structure and folding. *RNA*, **6**, 1672–1680.
33. Hargittai, M. R., Mangla, A. T., Gorelick, R. J. & Musier-Forsyth, K. (2001). HIV-1 nucleocapsid protein zinc finger structures induce tRNA(Lys,3) structural changes but are not critical for primer/template annealing. *J. Mol. Biol.* **312**, 985–997.
34. Flynn-Charlebois, A., Lee, N. & Suga, H. (2001). A single metal ion plays structural and chemical roles in an aminoacyl-transferase ribozyme. *Biochemistry*, **40**, 13623–13632.
35. Vaidya, A. & Suga, H. (2001). Diverse roles of metal ions in acyl-transferase ribozymes. *Biochemistry*, **40**, 7200–7210.
36. Kaye, N. M., Zahler, N. H., Christian, E. L. & Harris, M. E. (2002). Conservation of helical structure contributes to functional metal ion interactions in the catalytic domain of ribonuclease P RNA. *J. Mol. Biol.* **324**, 429–442.
37. Saito, H. & Suga, H. (2002). Outersphere and innersphere coordinated metal ions in an aminoacyl-tRNA synthetase ribozyme. *Nucl. Acids Res.* **30**, 5151–5159.
38. Kaukinen, U., Lyytikainen, S., Mikkola, S. & Lonnberg, H. (2002). The reactivity of phosphodiester bonds within linear single-stranded oligoribonucleotides is strongly dependent on the base sequence. *Nucl. Acids Res.* **30**, 468–474.
39. Bibillo, A., Figlerowicz, M., Ziomek, K. & Kierzek, R. (2000). The nonenzymatic hydrolysis of oligoribonucleotides. VII. Structural elements affecting hydrolysis. *Nucleosides Nucleotides Nucl. Acids*, **19**, 977–994.
40. Nakano, S., Proctor, D. J. & Bevilacqua, P. C. (2001). Mechanistic characterization of the HDV genomic ribozyme: assessing the catalytic and structural contributions of divalent metal ions within a multichannel reaction mechanism. *Biochemistry*, **40**, 12022–12038.
41. Cheong, C., Varani, G. & Tinoco, I., Jr (1990). Solution structure of an unusually stable RNA hairpin, 5′GGAC(UUCG)GUCC. *Nature*, **346**, 680–682.
42. Allain, F. H. & Varani, G. (1995). Structure of the P1 helix from group I self-splicing introns. *J. Mol. Biol.* **250**, 333–353.
43. Ennifar, E., Nikulin, A., Tishchenko, S., Serganov, A., Nevskaya, N., Garber, M. *et al.* (2000). The crystal structure of UUCG tetraloop. *J. Mol. Biol.* **304**, 35–42.
44. Feig, A. L., Panek, M., Horrocks, W. D., Jr & Uhlenbeck, O. C. (1999). Probing the binding of Tb(III) and Eu(III) to the hammerhead ribozyme using luminescence spectroscopy. *Chem. Biol.* **6**, 801–810.
45. Doudna, J. A. & Cech, T. R. (2002). The chemical repertoire of natural ribozymes. *Nature*, **418**, 222–228.

46. Moore, P. B. & Steitz, T. A. (2002). The involvement of RNA in ribosome function. *Nature*, **418**, 229–235.
47. Hannon, G. J. (2002). RNA interference. *Nature*, **418**, 244–251.
48. Nakano, S., Cerrone, A. L. & Bevilacqua, P. C. (2003). Mechanistic characterization of the HDV genomic ribozyme: classifying the catalytic and structural metal ion sites within a multichannel reaction mechanism. *Biochemistry*, **42**, 2982–2994.
49. Lafontaine, D. A., Ananvoranich, S. & Perreault, J. P. (1999). Presence of a coordinated metal ion in a *trans*-acting antigenomic delta ribozyme. *Nucl. Acids Res.* **27**, 3236–3243.
50. Tinsley, R. A., Harris, D. A. & Walter, N. G. (2003). Significant kinetic solvent isotope effects in folding of the catalytic RNA from the hepatitis delta virus. *J. Am. Chem. Soc.* **125**, 13972–13973.
51. Tinsley, 5.1., Harris, R. A., Walter, D. A. & Magnesium, N. G. (2004). dependence of the amplified conformational switch in the *trans*-acting hepatitis delta virus ribozyme. *Biochemistry*, in the press.
52. Matysiak, M., Wrzesinski, J. & Ciesiolka, J. (1999). Sequential folding of the genomic ribozyme of the hepatitis delta virus: structural analysis of RNA transcription intermediates. *J. Mol. Biol.* **291**, 283–294.
53. Murray, J. B., Seyhan, A. A., Walter, N. G., Burke, J. M. & Scott, W. G. (1998). The hammerhead, hairpin and VS ribozymes are catalytically proficient in monovalent cations alone. *Chem. Biol.* **5**, 587–595.
54. Antao, V. P., Lai, S. Y. & Tinoco, I., Jr (1991). A thermodynamic study of unusually stable RNA and DNA hairpins. *Nucl. Acids Res.* **19**, 5901–5905.
55. Mundoma, C. & Greenbaum, N. L. (2002). Sequestering of Eu(III) by a GAAA RNA tetraloop. *J. Am. Chem. Soc.* **124**, 3525–3532.
56. Scaringe, S. A. (2001). RNA oligonucleotide synthesis *via* 5′-silyl-2′-orthoester chemistry. *Methods*, **23**, 206–217.
57. Walter, N. G. (2001). Structural dynamics of catalytic RNA highlighted by fluorescence resonance energy transfer. *Methods*, **25**, 19–30.
58. Walter, N. G. (2002). Probing RNA structural dynamics and function by fluorescence resonance energy transfer (FRET). *Curr. Protocols Nucl. Acid Chem.* **11.10**, 11.10.1–11.10.23.
59. Wadkins, T. S. & Been, M. D. (1997). Core-associated non-duplex sequences distinguishing the genomic and antigenomic self-cleaving RNAs of hepatitis delta virus. *Nucl. Acids Res.* **25**, 4085–4092.
60. Marky, L. A. & Breslauer, K. J. (1987). Calculating thermodynamic data for transitions of any molecularity from equilibrium melting curves. *Biopolymers*, **26**, 1601–1620.

Edited by J. Doudna

(Received 1 April 2004; received in revised form 17 May 2004; accepted 19 May 2004)